

Engineering the impact of phonon dephasing on the coherence of a WSe₂ single-photon source via cavity quantum electrodynamics

Victor N. Mitryakhin,¹ Jens-Christian Drawer,¹ Hangyong Shan,¹ Alexander Steinhoff,² Matthias Florian,³ Lukas Lackner,¹ Bo Han,¹ Falk Eilenberger,⁴ Sefaattin Tongay,⁵ Kenji Watanabe,⁶ Takashi Taniguchi,⁷ Carlos Antón-Solanas,⁸ Ana Predojević,^{1,9} Christopher Gies,² Martin Esmann,¹ and Christian Schneider¹

¹*Institute of Physics, Carl von Ossietzky University of Oldenburg, 26129 Oldenburg, Germany*

²*Institute for Theoretical Physics and Bremen Center for Computational Material Science, University of Bremen, 28334 Bremen, Germany*

³*University of Michigan, Department of Electrical Engineering and Computer Science, Ann Arbor, Michigan 48109, USA*

⁴*Friedrich Schiller University Jena, Jena, Germany*

⁵*Materials Science and Engineering, School for Engineering of Matter, Transport and Energy, Arizona State University, Tempe, 85287, Arizona, USA*

⁶*Research Center for Functional Materials, National Institute for Materials Science, 1-1 Namiki, Tsukuba 305-0044, Japan*

⁷*International Center for Materials Nanoarchitectonics,*

National Institute for Materials Science, 1-1 Namiki, Tsukuba 305-0044, Japan

⁸*Depto. de Física de Materiales, Instituto Nicolás Cabrera,*

Instituto de Física de la Materia Condensada, Universidad Autónoma de Madrid, 28049 Madrid, Spain

⁹*Department of Physics, Stockholm University, 10691 Stockholm, Sweden*

(Dated: July 14, 2023)

Emitter dephasing is one of the key issues in the performance of solid-state single photon sources. Among the various sources of dephasing, acoustic phonons play a central role in adding decoherence to the single photon emission. Here, we demonstrate, that it is possible to tune and engineer the coherence of photons emitted from a single WSe₂ monolayer quantum dot via selectively coupling it to a spectral cavity resonance. We utilize an open cavity to demonstrate spectral enhancement, leveling and suppression of the highly asymmetric phonon sideband, finding excellent agreement with our microscopic theory. Most importantly, the impact of cavity tuning on the dephasing is directly assessed via optical interferometry, which clearly points out the capability to utilize light-matter coupling to steer and design dephasing and coherence of the emission properties of atomically thin crystals.

In contrast to excitations in isolated atoms, an appropriate understanding of the light-matter coupling of excitons in solid-state quantum emitters cannot be developed without considering the crucial impact of the lattice environment. Especially in the context of emission of quantum light, it is the coupling of excitons to acoustic phonons in most semiconductors and insulators that manifests via the formation of spectral side-bands and replica-like modes [1–3].

While such phenomena can be directly employed in quantum-optomechanic experiments [4–10], they typically impede the coherence of the emitted light fields in manners, which are uniquely material-specific. Atomically thin crystals belong to the most intriguing class of quantum materials utilized in modern photonic research [11]. Due to their ultimate thinness, the correlations of carriers are strongly enhanced and dominate their optical response. In the presence of random or engineered local strain, the formation of luminescent hot spots has been verified [12, 13], displaying non-classical light emission. Such quantum dots (QDs) can be found in the majority of thin-layer transition metal dichalcogenide (TMDC) crystals. However, they are particularly pronounced in WSe₂ monolayers and bilayers, which have been extensively studied in this regard [12, 14–17]. QDs in TMDCs have recently shifted into the spotlight of quantum photonic

research: In contrast to conventional quantum emitters in bulk material, two-dimensional QDs are highly tunable without the need for demanding semiconductor processing technologies [15, 18]. They can be conveniently integrated into photonic architectures without the restrictions of lattice matching [19], which can be realized via simple low-cost pick-and-place methods [20].

Despite this ease of integrating TMDC QDs into photonic devices, thus far, the enhancement of spontaneous emission from monolayer QDs has only been demonstrated in a limited number of reports. The Purcell-regime has been verified using TMDC-Bragg grating cavities [21], plasmonic structures [22–24], and most recently in tunable open-optical cavities [25].

Dephasing channels compromise and dictate the coherence of the emitted photons and are yet to be exhaustively studied. While it is possible to generally engineer crystal superlattices on the nano-scale to suppress coupling to phonons, such approaches are typically technologically too demanding to be implemented routinely [26–31]. Up to now, spectral wandering has been identified as one of the main sources of decoherence in the emission of 2D crystal QDs [32–34]. In addition, it was shown that due to the large Huang-Rhys factor of WSe₂, the coupling to phonons is extraordinarily strong and induces a very rich phonon-sideband spectrum [35].

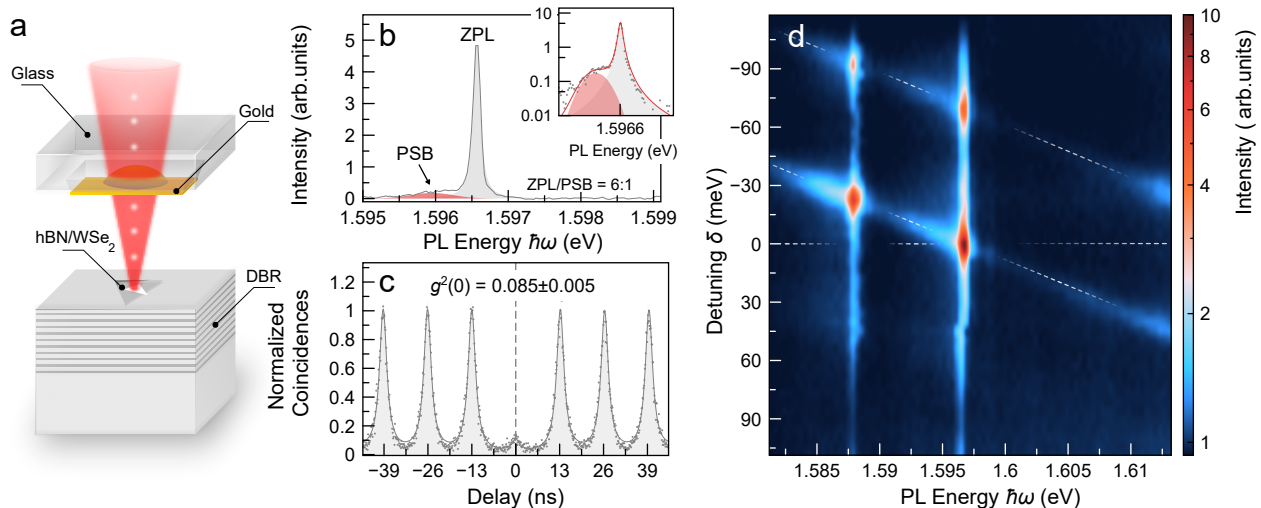


FIG. 1. (a) Schematics of an open cavity device under optical excitation. A beam is focused through the top concave mirror onto the monolayer exciting the QD dot and triggering the emission of single photons. The generated single photons escape the cavity through the top mirror. (b) PL spectrum of the quantum dot at 3.2 K recorded without the cavity top mirror. (c) Second-order correlation function. The separation of the peaks is inverse proportional to the laser repetition rate. The non-zero delay peaks have been fitted with an ensemble of Lorentzian functions. (d) Colormap showing PL spectra as a function of relative detuning of a cavity resonance from the emission energy. The intensity (color coded) is plotted in \log_{10} scale. The inclined dashed white lines indicate the cavity modes.

Here, we demonstrate that the unique shape of the phonon sideband in WSe₂ QDs can be exploited to engineer its coherence properties via emitter-cavity coupling. Specifically, by tuning the optical resonance of our cavity system to match either the zero-phonon emission line (ZPL) or the phonon sideband (PSB), we engineer the individual contributions of these two features of emission to the overall emission spectrum. As a result, the temporal coherence of the single photon emission can be controlled, changing from a slowly decaying single exponential trace to a double-exponential trace as the cavity resonance is tuned across the emission spectrum.

The WSe₂ QDs are coupled to an asymmetric plano-concave open cavity (depicted in Figure 1a). The cavity consists of two mirrors that are freely movable in three directions by means of xyz-nanopositioners. The bottom mirror is a highly reflective distributed Bragg reflector (DBR) composed of 10 SiO₂/TiO₂ layers grown on a SiO₂ substrate and features a stopband centered at 755 nm. A WSe₂ monolayer is placed onto the surface of the DBR via the dry-stamp method [20] and capped by hBN. The top mirror is composed of fused silica (SiO₂) that has been treated to have a square 100x100 μm^2 mesa in the center. In the mesa region, a lens of 5 μm diameter and 300 nm depth (the radius of curvature is 6.8 μm) is etched using focused ion beam milling. The top mirror is coated with a layer of gold (nominal thickness is 33 nm) via electron beam evaporation.

The mirrors separation is tuned within the range of 5 to 6 μm , which allows for high emission extraction [25].

The spectral cavity resonance has a full width at half maximum (FWHM) of 3.5 meV, which translates to a quality factor of 450. The device stack is placed into a low-vibration closed-cycle cryostat and held at a temperature of 3.2 K while being excited by a continuous wave Ti:Sapphire laser tuned at 1.722 eV (720 nm) and focused to an approximately 3 μm spot onto the gold surface of the top mirror in Figure 1a.

Prior to the studies of photoluminescence (PL) from the QD placed in the cavity, the QD emission (associated with localized excitons in a WSe₂ monolayer) without a cavity is investigated (see Figure 1b). In general, a PL spectrum of the WSe₂ QD features a pronounced ZPL and a lower energy PSB. In our case, Fig. 1b shows the ZPL spectrum located at 1.596 eV, with a linewidth of 110 ± 3 μeV (spectrometer resolution-limited). The linewidth of the PSB is 0.7 ± 0.1 meV. The ZPL and PSB are separated by 0.6 meV resulting in an asymmetric shape of the emission spectrum (see also the inset of Figure 1b, plotted in logarithmic scale).

To verify the single photon character of the PL emission, we implement a second-order correlation measurement (see Figure 1c), resulting in a $g^2(0) = 0.085 \pm 0.005$, which is significantly lower than previously reported for above-band driven WSe₂ QDs [24, 36]. This measurement is carried out in a resonant cavity-QD configuration, profiting from the significant signal enhancement.

The resonant enhancement of photon flux is a direct consequence of the modification of the emitter decay rate and light distribution in the cavity via the Purcell effect

[37]. The modification of the luminescence while sweeping the cavity resonance through the QD ZPL are shown in Fig. 1d. These PL spectra are plotted vs the cavity-emitter detuning $\delta = \hbar\omega_{cav} - \hbar\omega_0$, where $\hbar\omega_{cav}$ is the energy of a cavity resonance and $\hbar\omega_0$ is the ZPL energy (see Fig. 1d, and extracted PL spectra for several detunings in Fig. 2a). When the ZPL is in resonance with the cavity, the intensity of the emission is enhanced by more than a factor of 6 compared to the off-resonant case. The PSB is also notably affected by the cavity tuning: when the cavity is positively detuned, the contribution of the PSB to the PL spectrum is almost negligible and the ZPL is ultimately dominant. For the zero and negative detunings, the PSB contribution is notable and manifests itself as a distinct spectral feature in Figure 1d. We study this phenomenon to qualify the interplay between the ZPL and PSB integral intensities for cavity-emission tuning by applying a fitting procedure based on the independent boson model [38]. We include coupling of the local emitter to two-dimensional longitudinal acoustic phonons with matrix elements given in Ref. [39] and a localized phonon mode [40]. The optical susceptibility of the QD-phonon system is

$$\chi(t) = i\theta(t)e^{-i\omega_0 t + \Phi(t) - \Gamma_{inhom}^2 t^2} \quad (1)$$

with Γ_{inhom} being the inhomogeneous broadening, and the phonon dephasing integral

$$\Phi(t) = \sum_j \int_0^\infty d\omega \frac{J_j(\omega)}{\pi\omega^2} \left\{ \coth\left(\frac{\hbar\omega}{2k_B T}\right) [\cos(\omega t) - 1] - i\sin(\omega t) \right\}. \quad (2)$$

Here, $\hbar\omega$ is the PL energy, and $J_j(\omega)$ is the spectral density of phonon branch j . The corresponding emission spectrum is obtained by inverting the absorption spectrum at the ZPL:

$$I_{QD-PSB}(\omega) = \alpha(2\omega_0 - \omega) = \text{Im} \left\{ \int_{-\infty}^\infty dt \chi(t) e^{i(2\omega_0 - \omega)t} \right\}. \quad (3)$$

The cavity is explicitly accounted for in the model by multiplying the QD-sideband emission spectrum with a Lorentzian lineshape function:

$$I(\omega) = I_{QD-PSB}(\omega) \cdot \frac{a_{cav}/\gamma_{cav}}{\left(1 + \frac{(\omega - \omega_{cav})^2}{\gamma_{cav}^2}\right)} \quad (4)$$

Finally, we also account for an additive background emission I_{BG} . During the fitting procedure, we keep the emitter-phonon coupling parameters fixed for all detunings, allowing only the ZPL position, the cavity frequency, linewidth and the background contribution to

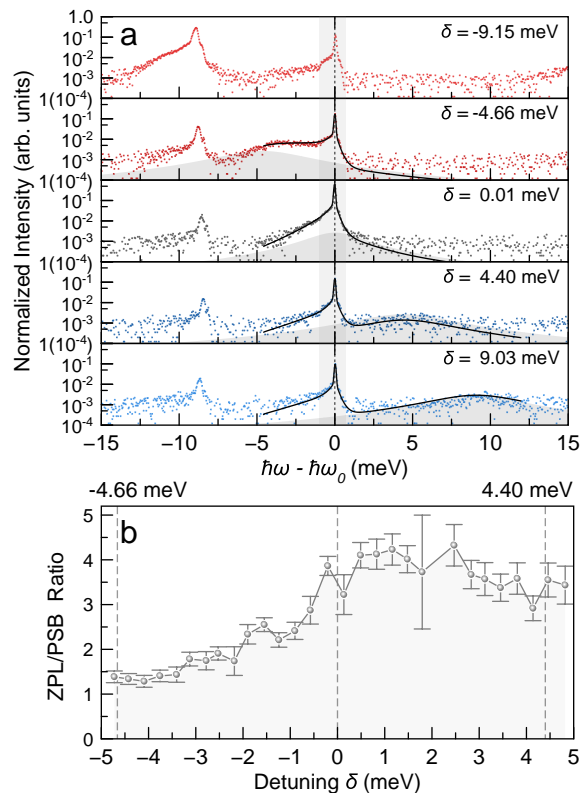


FIG. 2. (a) PL spectra for selected cavity-emitter detunings [-9.15, -4.60, 0.00, 4.60, 8.92] meV excited by the Ti:Sapphire laser in CW regime at 720 nm wavelength. The position of the cavity is indicated by the grey colored region. The solid black lines arise from the theoretical model. From the fit we obtain a lattice temperature of 3.9 K. (b) Ratio between the intensities of the ZPL and the PSB emission as the function of cavity-ZPL detuning.

change with varying detuning. The resulting spectral fittings are shown in four panels of Fig. 2a. For the lowest detuning (top panel), the cavity spectrally overlaps with the second QD (located at 1.5875 eV), which hinders fitting the spectrum.

While our model provides a numerically exact description of the emitter-phonon coupling and quantitatively explains all spectral features and their lineshapes, it does not allow us to quantify the ZPL/PSB contribution to the emission. Therefore, we extract the emission fraction of the ZPL and the PSB from experimental data by fitting the PL lineshape using a simplified model described in [41] (see Figure 2b). The PL spectra analysis quantifies the ZPL/PSB interplay: the resulting extracted ratio of the ZPL to the PSB is approximately 4 for the positively detuned cavity, which indicates a regime that is vastly dominated by the ZPL. In turn, for the negatively detuned case, it approaches unity. This suggests a tremendous impact of the PSB on the coherence of single photons emitted from the QD-cavity device under such detuning conditions. To account for the limits of con-

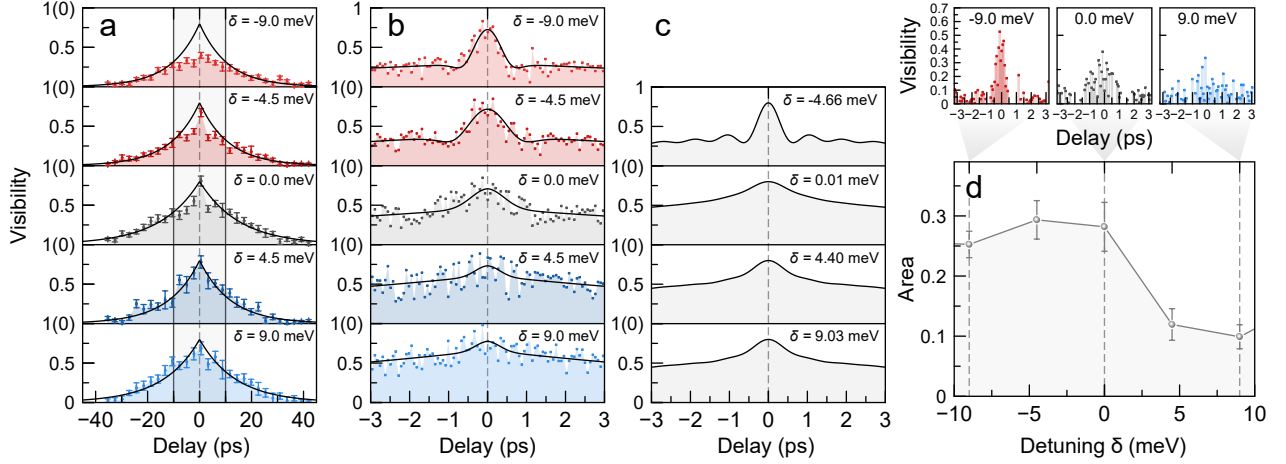


FIG. 3. Interference visibility data obtained using a Michelson interferometer: (a) for $[-40, 40]$ ps and (b) for $[-3.2, 3.2]$ ps range of values of the time delay between the arms of the interferometer. The visibility data is recovered from the interferograms, where the signal envelopes were extracted by fitting a sine function to the data for fixed x-axis intervals. Afterwards, for panel a, the visibility data is fitted. Since for longer time delays, the double exponential decay term in Eq. (7) becomes dominant, the fitting is performed disregarding the Gaussian decay term and excluding the range of $[-10, 10]$ ps (shown as shaded area in panel a), while locking the amplitude to the maximum observed value of 0.8. An average value of slow decay time scale τ_1 is extracted from the fits: 11.8 ± 0.4 ps. For panel b, the data is fitted with a function proportional to Eq. (7) while τ_1 is fixed to 11.8 ps. The resulting fits are plotted in black solid lines. (c) The visibility data calculated from Fourier transform of the fit from Figure 2a. (d) Area of the visibility (from which the slow decaying trace is subtracted) as function of the cavity-emission detuning. For the points corresponding to the detunings -9, 0 and 9 meV, the leftover fragment is plotted in separate panels on top and represents the contribution of the PSB to the overall interference visibility.

ventional spectroscopy and directly verify the impact of these phenomena on photon coherence, we extend our study to interferometric measurements in the time domain.

Within these studies, we filtered the QD-cavity emission using a 2.5 meV FWHM bandpass filter (which selects only the QD emission, see Figure 2a - the filtering FWHM is highlighted with a semi-transparent gray area) and conducted a set of first-order correlation function measurements using a Michelson interferometer, as we change the emitter-cavity detuning (see Figure 3a-b). Scanning the relative phase between the arms of the interferometer, we obtain interferograms displaying intensity oscillations. Yielding the value of the first order correlation function for a given temporal delay in the interferometer, the interference visibility of these oscillations is extracted as follows: $\text{Visibility} = (I_{max} - I_{min}) / (I_{max} + I_{min})$, where I_{max}/I_{min} is the upper/lower envelope of the interferogram signal, respectively.

In Fig. 3a, we plot the resulting extracted interference visibility as we scan our interferometer coarsely in steps corresponding to ≈ 2.5 ps. The measurements already reveal a tremendous influence of the emitter-cavity detuning on the first order coherence of the system. While all visibility traces decay with constant coherence time at longer time-scales, at very short time scales the interference visibilities for negative detunings are significantly

reduced and deviate from the simple exponential decay. This phenomenon is further investigated in Figure 3b, where we present several plots that show the visibility in the vicinity of the zero path difference between the two interferometer arms with much finer time resolution.

The visibility plots exhibit a pronounced fast decay that we can clearly associate with the contribution of the PSB (which is of Gaussian shape) to the emission spectrum, and the slowly decaying background that we attribute to the ZPL emission. Crucially, the impact of the pronounced fast decay clearly depends on the QD-cavity detuning, whereas the slow decay remains widely unaffected.

Since the interferograms display the temporal coherence profile of the emission, they are connected to the spectral shape of the emission via Fourier transformation. We can harness our fully microscopic model that was already used in Figure 2a and express the theoretical visibilities of photon coherence via Fourier transformation. To this end, we normalize $I(\omega) - I_{BG}$ to unity and evaluate

$$I(t) = \int_{\omega_{low}}^{\omega_{up}} d\omega (I(\omega) - I_{BG}) e^{i(\omega - \omega_0)t} \quad (5)$$

with integration limits such that the ZPL and the PSB are included: $\hbar\omega_{low} = \hbar\omega_0 - 5$ meV, $\hbar\omega_{up} = \hbar\omega_0 + 2$ meV.

For Fig. 3c, the cavity detuning is varied according

to the theoretical spectra shown in Fig. 2a. We find an overall good agreement with the experimentally obtained temporal coherence. As mentioned for the top panel in Fig. 2a, the impossibility to fit the spectrum prevents us from calculating the visibility in the most negative detuning (-9.15 meV). The signal shows the fastest decay for negative detuning, while zero and positive detunings lead to comparably long decay times. The most striking feature that cannot be extracted directly from the experimental data is the pronounced oscillation of the signal at negative detuning with a period of about 1 ps. We attribute this oscillation to an interference between the emitter and the cavity-enhanced PSB.

To further extent our quantitative analysis, we fit the experimental data with a function based on the Fourier transformation of a typical emission spectral shape of these QDs. We approximate the corresponding intensity of the signal recorded in the Michelson interferometer as:

$$I(t) = I_0 + \frac{A_1}{\tau_1} e^{-\frac{|t|}{\tau_1}} \cos(\omega_1 t) + \frac{A_2}{\tau_2} e^{-\frac{1}{\ln 2} \frac{t^2}{\tau_2^2}} \cos(\omega_2 t). \quad (6)$$

Here, t is the delay between the two arms of the interferometer, I_0 is the intensity of the signal at the input of the interferometer, and $A_{1,2}$, $\tau_{1,2}$, $\omega_{1,2}$ are the amplitudes, decay times and the frequencies of the individual components, respectively. The extraction of the envelopes is possible while considering the interference of two plane wave resulting in:

$$I_{max,min}(t) = I_0 \pm \left\{ \frac{A_1^2}{\tau_1^2} e^{-2\frac{|t|}{\tau_1}} + \frac{A_2^2}{\tau_2^2} e^{-\frac{2}{\ln 2} \frac{t^2}{\tau_2^2}} + 2A_1 A_2 \cdot e^{-\frac{|t|}{\tau_1}} e^{-\frac{1}{\ln 2} \frac{t^2}{\tau_2^2}} \cdot \cos(|\omega_1 - \omega_2|t) \right\}^{1/2}. \quad (7)$$

Since the upper and the lower envelopes are symmetric according to Eq. (7), the visibility trace is expressed as $Constant \cdot |I_{max}|$, which shows excellent agreement with the the experimental data (see Figure 3b).

Our fitting procedure reveals a coherence time associated with ZPL of approximately 11.8 ± 0.4 ps, which is consonant with the reported values for an essentially identically fabricated WSe₂ flake investigated under various temperatures. This value is furthermore consistent with the observed spectral linewidth of the ZPL of 110 μ eV. The fitting also gives a quantitative indication of the PSB contribution to the overall dephasing time of the emission as the function of cavity-emitter detuning. This contribution is most straightforwardly reflected by its relative area in the curves traces. We extract this area by first subtracting the slow decaying trace (the ZPL contribution) and repeat this method for every detuning. For the points corresponding to the detunings -9, 0 and 9 meV, the leftover fragment is plotted in separate panels on top and represents the contribution of the PSB to

the overall interference visibility. Strikingly, as shown in Figure 3d) the phonon impact on the first order temporal coherence is of great significance for negative as well as zero detuning conditions, but can almost be completely suppressed for positive detunings.

CONCLUSION

We provided a novel pathway to cavity-control the optical properties of quantum emitters in general, and WSe₂ QDs in particular. While previous works specifically utilized the coupling of QDs to optical cavities to enhance the photon flux, as well as to engineer the spontaneous emission lifetime, here, we verify that the cavity-emitter detuning directly influences the emitter coherence time (T_2). This significant effect is prominently exposed both in the spectral as well as in the temporal domain. The way to gain control of the emitter coherence utilizes selective enhancement of the emission of the zero phonon line versus the rapidly dephasing phonon sideband (which is unavoidable and material specific). Indeed, this method does not require high-Q cavities and works particularly well in the case of WSe₂ QDs featuring a very asymmetric phonon sideband, as we scrutinize within our microscopic and material-realistic theory. While our QDs still suffer from a rapidly dephased ZPL that sets limits to the overall temporal coherence, our methodology to engineer the impact of the phonon collisions on the coherence of the emitted light beam is universal. It will be possible to apply it to a next generation of WSe₂ QDs with reduced dephasing, possibly based on optimized crystals with advanced charge control as well as excited using resonant driving schemes, which will pave the way towards coherent TMDC single photon sources.

ACKNOWLEDGEMENTS

The authors acknowledge funding from the German federal ministry of education and research (BMBF) within the Projects ‘TUBLAN’ and ‘EQUAISE’. The project ‘EQUAISE’ was funded within the QuantERA program. S.T. acknowledges primary support from NSF DMR 2111812 for materials development, NSF GOALI 2129412 for scaling, and NSF ECCS 2111812 fabrication. We acknowledge partial support for DOE-SC0020653 (materials texture development), NSF ECCS 2052527 for electronic and NSF DMR 2206987 for magnetic purity tests. C.A.S. acknowledges the support from the Comunidad de Madrid fund “Atraccion de Talento, Mod. 1”, Ref. 2020-T1/IND-19785 and the project from the Ministerio de Ciencia e Innovación PID2020113445GB-I00. M.F. acknowledges support by the Alexander von Humboldt foundation. A. P. acknowledges the Helene

Lange Visiting Professorship program. M.E. acknowledges funding from the University of Oldenburg through a Carl von Ossietzky Young Researchers' Fellowship.

-
- [1] E. Stock, M.-R. Dachner, T. Warming, A. Schliwa, A. Lochmann, A. Hoffmann, A. I. Toropov, A. K. Bakarov, I. A. Derebezov, M. Richter, V. A. Haisler, A. Knorr, and D. Bimberg, Acoustic and optical phonon scattering in a single In(Ga)As quantum dot, *Phys. Rev. B* **83**, 041304 (2011).
- [2] C. Galland, A. Högele, H. E. Türeci, and A. m. c. Imamoğlu, Non-markovian decoherence of localized nanotube excitons by acoustic phonons, *Phys. Rev. Lett.* **101**, 067402 (2008).
- [3] T. Grange, N. Somaschi, C. Antón, L. De Santis, G. Coppola, V. Giesz, A. Lemaître, I. Sagnes, A. Auffèves, and P. Senellart, Reducing phonon-induced decoherence in solid-state single-photon sources with cavity quantum electrodynamics, *Phys. Rev. Lett.* **118**, 253602 (2017).
- [4] S. Barzanjeh, A. Xuereb, S. Groeblacher, M. Paternostro, C. A. Regal, and E. M. Weig, Optomechanics for quantum technologies, *Nature Physics* **18**, 15 (2022).
- [5] M. Aspelmeyer, T. J. Kippenberg, and F. Marquardt, Cavity optomechanics, *Rev. Mod. Phys.* **86**, 1391 (2014).
- [6] Y. Chu, P. Kharel, T. Yoon, L. Frunzio, P. T. Rakich, and R. J. Schoelkopf, Creation and control of multi-phonon fock states in a bulk acoustic-wave resonator, *Nature* **563**, 666 (2018).
- [7] J. Kettler, N. Vaish, L. M. de Lepinay, B. Besga, P.-L. de Assis, O. Bourgeois, A. Auffèves, M. Richard, J. Claudon, J.-M. Gerard, B. Pigeau, O. Arcizet, P. Verlot, and J.-P. Poizat, Inducing micromechanical motion by optical excitation of a single quantum dot, *Nature Nanotechnology* **16**, 283 (2021).
- [8] M. Weiß, D. Wigger, M. Nägele, K. Müller, J. J. Finley, T. Kuhn, P. Machnikowski, and H. J. Krenner, Optomechanical wave mixing by a single quantum dot, *Optica* **8**, 291 (2021).
- [9] J.-M. Pirkkalainen, S. U. Cho, F. Massel, J. Tuorila, T. T. Heikkilä, P. J. Hakonen, and M. A. Sillanpää, Cavity optomechanics mediated by a quantum two-level system, *Nature Communications* **6**, 6981 (2015).
- [10] M. Montinaro, G. Wuest, M. Munsch, Y. Fontana, E. Russo-Averchi, M. Heiss, A. Fontcuberta i Morral, R. J. Warburton, and M. Poggio, Quantum dot opto-mechanics in a fully self-assembled nanowire, *Nano Letters* **14**, 4454 (2014), pMID: 25010118, <https://doi.org/10.1021/nl501413t>.
- [11] C. hua Liu, J. Zheng, Y. Chen, T. Fryett, and A. Majumdar, Van der waals materials integrated nanophotonic devices (invited), *Opt. Mater. Express* **9**, 384 (2019).
- [12] Y.-M. He, G. Clark, J. R. Schaibley, Y. He, M.-C. Chen, Y.-J. Wei, X. Ding, Q. Zhang, W. Yao, X. Xu, C.-Y. Lu, and J.-W. Pan, Single quantum emitters in monolayer semiconductors, *Nature Nanotechnology* **10**, 497 (2015), number: 6 Publisher: Nature Publishing Group.
- [13] A. Branny, S. Kumar, R. Proux, and B. D. Gerardot, Deterministic strain-induced arrays of quantum emitters in a two-dimensional semiconductor, *Nature Communications* **8**, 15053 (2017).
- [14] M. Koperski, K. Nogajewski, A. Arora, V. Cherkez, P. Mallet, J.-Y. Veuillen, J. Marcus, P. Kossacki, and M. Potemski, Single photon emitters in exfoliated WSe₂ structures, *Nature Nanotechnology* **10**, 503 (2015), number: 6 Publisher: Nature Publishing Group.
- [15] C. Chakraborty, L. Kinnischtzke, K. M. Goodfellow, R. Beams, and A. N. Vamivakas, Voltage-controlled quantum light from an atomically thin semiconductor, *Nature Nanotechnology* **10**, 507 (2015), number: 6 Publisher: Nature Publishing Group.
- [16] A. Srivastava, M. Sidler, A. V. Allain, D. S. Lembke, A. Kis, and A. Imamoğlu, Optically active quantum dots in monolayer WSe₂, *Nature Nanotechnology* **10**, 491 (2015), number: 6 Publisher: Nature Publishing Group.
- [17] P. Tonndorf, R. Schmidt, R. Schneider, J. Kern, M. Buscema, G. A. Steele, A. Castellanos-Gomez, H. S. J. v. d. Zant, S. M. d. Vasconcellos, and R. Bratschkitsch, Single-photon emission from localized excitons in an atomically thin semiconductor, *Optica* **2**, 347 (2015), publisher: Optica Publishing Group.
- [18] O. Iff, D. Tedeschi, J. Martín-Sánchez, M. Moczala-Dusanowska, S. Tongay, K. Yumigeta, J. Taboada-Gutiérrez, M. Savaresi, A. Rastelli, P. Alonso-González, S. Höfling, R. Trotta, and C. Schneider, Strain-Tunable Single Photon Sources in WSe₂ Monolayers, *Nano Letters* **19**, 6931 (2019), publisher: American Chemical Society.
- [19] M. Turunen, M. Brotons-Gisbert, Y. Dai, Y. Wang, E. Scerri, C. Bonato, K. Jöns, Z. Sun, and B. Gerardot, Quantum photonics with layered 2d materials, *Nature Reviews Physics* **4**, 219 (2022).
- [20] A. Castellanos-Gomez, M. Buscema, R. Molenaar, V. Singh, L. Janssen, H. S. J. van der Zant, and G. A. Steele, Deterministic transfer of two-dimensional materials by all-dry viscoelastic stamping, *2D Materials* **1**, 011002 (2014).
- [21] O. Iff, Q. Buchinger, M. Moczala-Dusanowska, M. Kamp, S. Betzold, M. Davanco, K. Srinivasan, S. Tongay, C. Antón-Solanas, S. Höfling, and C. Schneider, Purcell-enhanced single photon source based on a deterministically placed WSe₂ monolayer quantum dot in a circular bragg grating cavity, *Nano Letters* **21**, 4715 (2021).
- [22] L. N. Tripathi, O. Iff, S. Betzold, L. Dusanowski, M. Emmerling, K. Moon, Y. J. Lee, S.-H. Kwon, S. Höfling, and C. Schneider, Spontaneous emission enhancement in strain-induced WSe₂ monolayer-based quantum light sources on metallic surfaces, *ACS Photonics* **5**, 1919 (2018).
- [23] T. Cai, J.-H. Kim, Z. Yang, S. Dutta, S. Aghaeimeibodi, and E. Waks, Radiative Enhancement of Single Quantum Emitters in WSe₂ Monolayers Using Site-Controlled Metallic Nanopillars, *ACS Photonics* **5**, 3466 (2018), publisher: American Chemical Society.
- [24] Y. Luo, G. D. Shepard, J. V. Ardelean, D. A. Rhodes, B. Kim, K. Barmak, J. C. Hone, and S. Strauf, Deterministic coupling of site-controlled quantum emitters in monolayer WSe₂ to plasmonic nanocavities, *Nature Nanotechnology* **13**, 1137 (2018).
- [25] J.-C. Drawer, V. N. Mitryakhin, H. Shan, S. Stephan, M. Gittinger, L. Lackner, B. Han, G. Leibeling, F. Eilenberger, R. Banerjee, S. Tongay, K. Watanabe, T. Taniguchi, C. Lienau, M. Silies, C. Anton-Solanas, M. Esmann, and C. Schneider, Ultra-bright single photon source based on an atomically thin material (2023), arXiv:2302.06340.

- [26] V. Narayanamurti, H. L. Störmer, M. A. Chin, A. C. Gossard, and W. Wiegmann, Selective transmission of high-frequency phonons by a superlattice: The "dielectric" phonon filter, *Phys. Rev. Lett.* **43**, 2012 (1979).
- [27] M. Trigo, A. Bruchhausen, A. Fainstein, B. Jusserand, and V. Thierry-Mieg, Confinement of acoustical vibrations in a semiconductor planar phonon cavity, *Phys. Rev. Lett.* **89**, 227402 (2002).
- [28] P. Santos, M. Hundhausen, and L. Ley, Observation of folded-zone acoustical phonons by raman scattering in amorphous Si-SiN_x superlattices, *Phys. Rev. B* **33**, 1516 (1986).
- [29] B. Jusserand, F. m. c. Alexandre, J. Dubard, and D. Paquet, Raman scattering study of acoustical zone-center gaps in GaAs/AlAs superlattices, *Phys. Rev. B* **33**, 2897 (1986).
- [30] B. Jusserand and M. Cardona, Raman spectroscopy of vibrations in superlattices, in *Light Scattering in Solids V: Superlattices and Other Microstructures*, edited by M. Cardona and G. Güntherodt (Springer Berlin Heidelberg, Berlin, Heidelberg, 1989) pp. 49–152.
- [31] M. Cazayous, J. Groenen, J. R. Huntzinger, A. Mlayah, and O. G. Schmidt, Spatial correlations and raman scattering interferences in self-assembled quantum dot multilayers, *Phys. Rev. B* **64**, 033306 (2001).
- [32] B. Spokoyny, H. Utzat, H. Moon, G. Grosso, D. Englund, and M. G. Bawendi, Effect of spectral diffusion on the coherence properties of a single quantum emitter in hexagonal boron nitride, *The Journal of Physical Chemistry Letters* **11**, 1330 (2020), pMID: 32017564, <https://doi.org/10.1021/acs.jpcllett.9b02863>.
- [33] S. White, C. Stewart, A. S. Solntsev, C. Li, M. Toth, M. Kianinia, and I. Aharonovich, Phonon dephasing and spectral diffusion of quantum emitters in hexagonal boron nitride, *Optica* **8**, 1153 (2021).
- [34] M. Brotons-Gisbert, A. Branny, S. Kumar, R. Picard, R. Proux, M. Gray, K. S. Burch, K. Watanabe, T. Taniguchi, and B. D. Gerardot, Coulomb blockade in an atomically thin quantum dot coupled to a tunable Fermi reservoir, *Nature Nanotechnology* **14**, 442 (2019).
- [35] Z.-W. Wang, Y. Xiao, J.-P. Deng, Y. Cui, and Z.-Q. Li, Multiphonon raman scattering mediated by the exciton states in monolayer transition metal chalcogenides, *Phys. Rev. B* **100**, 125308 (2019).
- [36] L. Sortino, P. G. Zotev, C. L. Phillips, A. J. Brash, J. Cambiasso, E. Marensi, A. M. Fox, S. A. Maier, R. Sapienza, and A. I. Tartakovskii, Bright single photon emitters with enhanced quantum efficiency in a two-dimensional semiconductor coupled with dielectric nanoantennas, *Nature Communications* **12**, 6063 (2021).
- [37] E. M. Purcell, Spontaneous Emission Probabilities at Radio Frequencies, in *Confined Electrons and Photons: New Physics and Applications*, edited by E. Burstein and C. Weisbuch (Springer US, Boston, MA, 1995) pp. 839–839.
- [38] C. B. Duke and G. D. Mahan, Phonon-broadened impurity spectra. i. density of states, *Phys. Rev.* **139**, A1965 (1965).
- [39] J. Klein, M. Lorke, M. Florian, F. Sigger, L. Sigl, S. Rey, J. Wierzbowski, J. Cerne, K. Mueller, E. Mitterreiter, P. Zimmermann, T. Taniguchi, K. Watanabe, U. Wurstbauer, M. Kaniber, M. Knap, R. Schmidt, J. J. Finley, and A. W. Holleitner, Site-selectively generated photon emitters in monolayer MoS₂ via local helium ion irradiation, *Nature Communications* **10**, 2755 (2019).
- [40] D. Wigger, R. Schmidt, O. D. Pozo-Zamudio, J. A. Preuss, P. Tonndorf, R. Schneider, P. Steeger, J. Kern, Y. Khodaei, J. Sperling, S. M. de Vasconcelos, R. Bratschitsch, and T. Kuhn, Phonon-assisted emission and absorption of individual color centers in hexagonal boron nitride, *2D Materials* **6**, 035006 (2019).
- [41] M. Abbarchi, M. Gurioli, A. Vinattieri, S. Sanguinetti, M. Bonfanti, T. Mano, K. Watanabe, T. Kuroda, and N. Koguchi, Phonon sideband recombination kinetics in single quantum dots, *Journal of Applied Physics* **104**, 10.1063/1.2948932 (2008), 023504.